

Nonlinear Finite Element Analysis of Critical Gusset Plates in the I-35W Bridge in Minnesota

Minmao Liao¹; Taichiro Okazaki, A.M.ASCE²; Roberto Ballarini, M.ASCE³;

Arturo E. Schultz, M.ASCE⁴; and Theodore V. Galambos, H.M.ASCE⁵

Abstract: Reported evidence suggests that failure of gusset plates initiated the collapse of the I-35W Bridge in Minneapolis, Minnesota. The particular gusset plates were at a panel point designated as U10. Therefore, an analytical investigation was conducted on the condition of the U10 gusset plates at the time of bridge collapse. The forces delivered to panel point U10 were reproduced using available information of the bridge. These forces were introduced to detailed nonlinear, three-dimensional finite element models to calculate stress and strain states of the gusset plates. The results indicate that substantial portions of the U10 gusset plates were yielded at the time of collapse, confirming earlier findings from federal and state investigations. Weight increase due to past deck reconstruction and construction material and equipment staged on the day of collapse, along with insufficient thickness of the gusset plate, were identified as the main contributing factors to the substantial yielding. The results also suggest that the interaction of compression and shear played an important role in the gusset plate failure.

Subject Headings: Bridge failure; Connections; Finite element method; Nonlinear analysis.

¹ Graduate Student, Department of Civil Engineering, University of Minnesota, Minneapolis, MN 55455.

² Research Fellow, E-Defense, National Research Institute for Earth Science and Disaster Prevention, Miki, Hyogo 673-0515, Japan .

³ Professor, Department of Civil Engineering, University of Minnesota, Minneapolis, MN 55455

⁴ Professor, Department of Civil Engineering, University of Minnesota, Minneapolis, MN 55455 (corresponding author e-mail: aeschultz@umn.edu).

⁵ Professor Emeritus, Department of Civil Engineering, University of Minnesota, Minneapolis, MN 55455.

Introduction

On Wednesday, August 1, 2007, the bridge carrying Interstate Highway 35W (I-35W) over the Mississippi river in Minneapolis, Minnesota, collapsed within a matter of seconds. The collapse of a highway bridge in a major U.S. downtown area was unprecedented. What makes the event peculiar is that the bridge was a very typical structure and that the collapse occurred under what was thought to be normal operating conditions except for minor deck, joint, lighting, and guardrail repairs. The longer spans of the bridge were constructed as a deck-truss bridge. Steel truss bridges such as the I-35W Bridge are a very common form for long-span bridges in the U.S. and worldwide. Until the event occurred, steel truss bridges had earned the reputation of being economical and reliable. While the small redundancy of the trusses may be of concern, it is believed that mandated maintenance procedures assure that this structural system is as safe and reliable as any other. Forensic evidence from the I-35W Bridge after collapse (Hill et al. 2008; NTSB 2009a; 2008e) suggests that the bridge failure initiated at gusset plates that connected the top chord members to a compression diagonal and tension diagonal. Holt and Hartmann (2008) suggest that the strength of the gusset plates was insufficient to develop the shear forces expected at this panel point.

Gusset plates are designed for the stresses at the Whitmore section (Whitmore 1952), block shear in tension, buckling in compression, and stresses calculated based on simple beam equations, in addition to constructability considerations (Gross 1990; Kulicki et al. 2006). The design rules are supported, in part, by laboratory tests by Bjorhovde and Chakrabarti (1985), Hardash and Bjorhovde (1985), Yam and Cheng (1993). In addition, analytical studies by Thornton (1984) and Gross (1990) address design approaches for gusset plate connections in building frames. However, these earlier studies have focused mainly on gusset plate connections

designed for tension and/or compression behavior, as seen in braced frames for building systems. Recently, Chambers and Ernst (2005) published a literature review on the design of gusset plate connections in braced building frames. However, little research data is available on gusset plates in truss bridge systems, where the gusset plates may connect multiple diagonal members and chord members.

The stress distribution in gusset plates for bridge trusses differs substantially from that in simple tension or compression connections, and varies with member arrangement. To the knowledge of the authors, the only tests of realistic gusset plate connections in truss bridge systems, conducted to date, are those sponsored by the Honshu-Shikoku Bridge Authority in preparation of major bridge construction in Japan. Yamamoto et al. (1985) examined the elastic stress distribution in gusset plates for a range of member arrangements, and used experimental data to develop refined, allowable stress design criteria for the thickness of gusset plates. Subsequently, Yamamoto et al. (1988) subjected gusset plate connection specimens to failure to determine their inelastic buckling strength. In a separate study, also sponsored by the Authority, Tajima et al. (1982) tested a number of large-scale specimens to improve gusset plate designs for fatigue performance. Although these studies provide valuable data on gusset plate connection behavior, they do not address fracture of gusset plates such as that observed in the I-35W Bridge.

In view of the above, an analytical study was conducted on the critical gusset plates in the collapsed I-35W Bridge (Liao 2009). Based on available information, the loading condition of the bridge at the time of collapse was estimated. A bridge model was used to evaluate truss forces, which were in turn, used in a detailed, finite element model of the critical gusset plate connection. The finite element modeling procedure was validated using available experimental data on tension and compression gusset plate connections. Results from the finite element

analyses were used to gain insight into possible causes of the gusset plate failure and possible collapse mechanisms.

Reported Facts

According to the Minnesota Department of Transportation (Mn/DOT 2008) and the NTSB (2008b; 2008e), construction of the I-35W Bridge began in 1964, and the bridge opened to traffic in 1967. The bridge had 14 spans and 13 piers including the south approach spans, north approach spans, and central deck-truss spans. Total length from abutment to abutment was 581 m. Fig. 1 shows a plan and elevation of the entire bridge, drawn based on original construction drawings released by the Mn/DOT (2008). The south and north approach spans rested at the ends of the two (west and east) main trusses, at panel points U0 and U0', respectively. The main truss rested on roller supports at piers 5, 6, and 8, and a hinge support at pier 7. The main truss consisted of 28 panels, each of which was 11.6 m long. The two main trusses were connected by floor trusses that spanned transversely between panel points. The floor trusses supported longitudinal stringers, which in turn supported the reinforced concrete deck and traffic, and a special detail was used at the connection between the stringer and main truss to transfer only gravity effects. Underneath the floor trusses, sway frames in a chevron configuration connected the two main trusses. The main trusses were also connected by lateral bracing spanning between the upper chords and lower chords. The deck was separated for the southbound and northbound traffic. Each deck accommodated four 3.7-m traffic lanes and two 0.6-m shoulders. The original concrete deck was designed as 165-mm thick, but the thickness was increased by 50 mm by concrete overlay added in later years. Outside barriers and median railings were also added to address maintenance and operational issues. At the time of collapse, a bridge patching and overlay project had been underway since June of 2007. Two southbound

inside lanes and two northbound outside lanes were closed for traffic. Construction material and equipment were staged on the closed southbound traffic lanes near the suspected location of failure initiation.

After the bridge collapsed, field investigations were conducted by the Mn/DOT and the NTSB. Reported observations (Hill et al. 2008; NTSB 2008c; NTSB 2008e) indicate that the failure initiated at panel point U10. Fig. 2(a) is a photograph taken prior to the collapse (NTSB 2008c), showing a pair of gusset plates connecting five truss members at panel point U10 of the west main truss (U10W). Fig. 2(b) identifies the five truss members: upper chords U9/U10 and U10/U11, diagonals L9/U10 and U10/L11, and a vertical U10/L10. The five truss members were connected through a pair of 13-mm thick gusset plates of ASTM A441 grade 50 steel (Beshah et al. 2008) and using 25-mm diameter rivets. The upper chords U9/U10 and U10/U11 and compression diagonal L9/U10 were box sections, while the tension diagonal U10/L11 and vertical U10/L10 were W-sections. All members were welded built-up sections. Because U10 was located near an inflection point of the continuous truss, the force in the upper chord switched from tension on one side of the panel point to compression on the other side, as indicated in Fig. 2(b), while the diagonal members delivered substantial compression and tension to the connection. As a result, a large net shear force was produced along the horizontal critical section indicated in the figure. Based on commonly used, simplified design checks, Holt and Hartmann (2008) suggested that the gusset plates at panel points U10 needed to be twice as thick to safely transfer the shear force produced by design loads.

Fig. 3(a) shows a photograph of panel point U10W taken after the collapse (NTSB 2008c), while Fig. 3(b) illustrates the three primary fractures seen in Fig. 3(a) and that were commonly observed in all four U10W and U10E gusset plates:

(A) Diagonal fracture along rivet holes connecting the gusset plate to the compression diagonal L9/U10. The fracture occurred along the perimeter holes of the rivet group adjacent to U10/L10.

(B) Horizontal fracture below the lower edge of upper chord U9/U10.

(C) Vertical fracture near the separation between the upper chords U9/U10 and U10/U11.

Fracture of gusset plates was uniquely observed in the U10 panel points. This observation combined with the fact that the design strength of the U10 gusset plates was insufficient to carry the design forces (Holt and Hartmann 2008) strongly suggest that failure of the I-35W Bridge initiated in the U10 gusset plates.

Load Estimation

Based on construction and reconstruction plans (Mn/DOT 2008), and vehicle, construction material, equipment loads, and weather report data (NTSB 2007), the loading condition of the bridge at the time of collapse was estimated as having the following five components:

- DL1: Dead loads at the time of original construction including the weight of all concrete and steel components. The original thickness of the concrete deck was 165 mm.
- DL2: Net increase in dead loads due to repair and reconstruction in 1977 and 1998 (Mn/DOT 2008). Added components included a 50-mm overlay on the concrete deck and new concrete parapets.
- LL: Live loads including vehicle loads and impact effects. The vehicle loads were evaluated by uniformly distributing the total vehicle weight present at the time of collapse, as reported by the NTSB (2007). Per specifications (AASHTO 1973), impact effects were accounted for by adding 30% of the vehicle loads to the live loads.

- CL: Construction loads. At the time of collapse, four piles of coarse aggregate (gravel), four piles of fine aggregate (sand), one water truck, one cement tanker, and one concrete mixer were placed near panel point U10 in preparation of deck paving operation (NTSB 2007). The total weight of the material and equipment was estimated as 262 tons.
- TH: Thermal effects, which were examined as two separate components: a uniform change in temperature due to daily change in ambient temperature and a temperature gradient expected in the immediate vicinity of the U10 panel point due to solar radiation. The former was modeled based on the peak-to-peak difference in ambient temperature on the day of collapse, which was reported to be 11 °C (NTSB 2007). The latter was estimated as 17 °C based on temperature monitored from a similar truss bridge in Cleveland, Ohio on October 11th, 1998 (Huckelbridge 2008). Unlike the other effects, temperature gradient was studied only in the local model analysis.

Table 1 lists the estimated loads on each of the main trusses at each panel point. Panel point designations are indicated in Fig. 1. The load values were obtained based on a tributary area calculation and assuming that the loads were shared evenly between the two main trusses. Loads on the south and north-end panel points (U0 and U0') include the loads transferred from the approach spans. The table shows that the dead loads added during deck reconstruction (DL2) were on the order of 30% of the original dead loads (DL1). This increment is quite significant. The vehicle load and impact effects combined (LL) was less than 6% of DL1 (of which approximately 1% was due to impact loading). The LL may have doubled if one-half of the traffic lanes had not been closed for traffic. Therefore, the live loads may have been a minor factor to the bridge collapse, and impact loading was of little consequence. Construction loads

(CL) were applied only on panel points U9 through U14. The CL added on U10 was greater than 20% of DL1.

Bridge Model Analysis

In order to study the overall response of the bridge, a 2D bridge model was constructed and analyzed using SAP 2000 version 11.0.8 (CSI 2007). The model geometry was based on the original construction drawings (Mn/DOT 2008). All member ends were assumed to be pinned. The support conditions were the same as designed, unless noted otherwise. Generic elastic properties of steel were assigned to the members. The deck was assumed not to act in a composite manner with the trussed for several reasons. The decks for the northbound and southbound lanes were separate, the deck was designed and built as a non-composite element (i.e., few shear connectors between deck and the stringers), and the patching operation introduced cutbacks and numerous perforations in the deck.

Fig. 4 shows the plot of influence lines for the truss forces (positive in tension) in the compression diagonal L9/U10 and tension diagonal U10/L11. The influence lines indicate that loads applied on the center span produces compression in L9/U10 and tension in U10/L11, and that loads placed near U10 produce a very large response. Therefore, the temporary construction loads (CL), which were placed in the shaded region of Fig. 4, may have significantly affected the forces imposed on the U10 gusset plate.

The loads listed in Table 1 were applied on the upper chord panel points of the model according to the following four combinations:

- Case 1: DL1
- Case 2: DL1 + DL2
- Case 3: DL1 + DL2 + LL

- Case 4: DL1 + DL2 + LL + CL

In addition, the following two cases were considered for the effect of uniform change in temperature.

- Case T1: Ambient temperature increase of 11 °C with as-designed support conditions
- Case T2: Ambient temperature increase of 11 °C with hinge supports used at all four piers.

This case addressed the extreme effects of frozen roller supports reported by URS (2006).

Table 2 lists the axial forces (positive in tension) in the truss members framing into U10. The dead load effects (corresponds to Case 1) and strength demand used in the original design are also listed for comparison. The forces computed for Case 4 are indicated in Fig. 2(b). The dead load effects agree well between the original design and estimation in this study, which suggests that the estimated dead loads (DL1) listed in Table 1 are reliable. The forces in Case 3 are smaller than the design strength demand, primarily because the design live loads prescribed by AASHTO (1973) is roughly 10 times greater than the live loads present at the time of bridge collapse. While analysis predicts minimal forces (62 kN for Case 4) in member U10/L10, this member was designed for a much larger force of 2,400 kN, perhaps in order to account for forces during construction of the bridge and accidental loading cases.

The deck repair in later years (DL2) increased the truss forces by 30%. Live loads (LL) and construction loads (CL) increased the truss forces by another 10 to 15%. The forces produced in the diagonals L9/U10 and U10/L11 by Case 4, which represent the total estimated load on the bridge at the time of collapse, exceed the design total effects by 5%. Forces computed for Case T1 are negligible compared to the forces for Case 4. Case T2 produces tension in member L9/U10 and compression in U10/L11. Therefore, if the roller supports were frozen, it is likely that increase in ambient temperature relaxed the compression in member

L9/U10, tension in member U10/L11, and shear force along the critical section shown in Fig. 2(b).

Validation of Finite Element Models

The finite element modeling procedure for the U10 gusset plate connection was established by simulating the laboratory test behavior of two, gusset plate connections. ABAQUS 6.8-1 (Simulia 2008) was used for all finite element analyses presented in this paper. Nonlinear material behavior was modeled using the von Mises yield criterion and the isotropic hardening rule. A large strain-large displacement formulation, which is the default option for ABAQUS, was used to carry out the nonlinear analysis. For the validation studies discussed in the following, the steel was modeled using the respective reported yield strength and a post-yield stiffness of approximately 0.01 times the Young's modulus.

The first validation used a bolted tension connection reported by and designated as Specimen 28 by Hardash and Bjorhovde (1985). This connection exhibited a long yield plateau leading to a tensile strength of 560 kN, and ultimately failed by block shear failure of the gusset plate. Fig. 5(a) shows the gusset plate after testing, where tensile fracture across the last row of bolts and elongation of bolt holes is visible. The finite element model of the gusset plate is shown in Fig. 5(b) as the global model. Considering symmetry, only one half of the gusset plate was modeled. All nodes along the left edge of the model were restrained against translation in two transverse (X and Z) directions. All nodes at the bottom edge of the plate were restrained against translation in all three (X, Y, and Z) directions. The bolts were modeled as rigid cylindrical shells. The rigid shells were displaced equally in the upward (positive Y) direction to deliver load to the gusset plate. The remaining five degrees-of-freedom of the rigid shells were restrained.

A comparison study of element types and mesh refinement led to the conclusion that the overall behavior of these connections may be modeled appropriately by using C3D8 elements and 16 elements surrounding the bolt holes. For example, Fig. 6(a) compares the loading curve obtained from using different solid elements, designated as C3D8 (linear isoparametric brick element), C3D8R (linear brick element with reduced integration), and C3D4 (linear isoparametric tetrahedral element) in the ABAQUS element library. All analyses used a similar meshing strategy with 16 nodes surrounding each bolt hole. The models using C3D8 or C3D8R achieved the measured strength of 560 kN at 10 mm displacement (after the bolts contacted the hole perimeter), and continued to develop larger strength. The strength degradation observed in the experiment was influenced by fracture propagation between the last row of bolts. Therefore, the discrepancy between the experiment and analysis may be attributed to absence of a fracture model in the analysis. The model using C3D4 exceeded the measured strength at a much smaller deformation of 4 mm, and was therefore judged as less appropriate than the other two models. Fig. 5(c) shows the deformation of the gusset plate and the Mises stress distribution when the bolts were displaced by 10 mm. Overall, the computed deformation and stress distributions and the photograph of the test specimen in Fig. 5(a) share several important similarities: Very high stresses were computed near the bearing side of the bolt holes, and also across the last row of bolt holes where fracture was observed in the test. In addition, deformation of the plate was supplied by bolt hole elongation, most notably at the last bolt hole.

In order to examine the critical stress and strain condition that led to fracture of the gusset plate, a densely meshed model representing the region surrounding the last row of bolt hole, shown in Fig. 5(b) as the submodel, was analyzed using the submodeling technique (Simulia 2008). The displacement field obtained from the global model was used as boundary conditions

for the submodel analysis. Fig. 6(b) and (c) plot the distribution of normal stress, σ_{YY} , and equivalent plastic strain, PEEQ, respectively, along the sampling line connecting the two bolt holes. The abscissa indicates the distance measured from the middle of the plate. The figure compares the results from the global model and submodel when the bolts were displaced by 10 mm (the loading stage when the measured strength was reached). The figures indicate that the yield strength (229 MPa) was exceeded along the entire length between the last row of bolts. Both σ_{YY} and PEEQ were largest at the edge of the bolt hole. The major difference between the global model and submodel occurs only near the edge of the bolt holes, where the global model does not capture the severe stress and strain concentration. The very large stress concentration obtained from the submodel indicates that fracture may initiate at the edge of the bolt hole at a load much lower than the tensile capacity of the gusset plate connection.

The second validation study used a bolted compression connection reported by Yam and Cheng (1993) and designates as specimen SP1. The gusset plate had a slender, 725-mm long and 13.3-mm thick, unbraced edge. The brace member delivering compression was restrained from torsion and rotation in the plane perpendicular to the gusset plate. The bottom edges of the gusset plate were fixed, while the base support was permitted to translate only in the out-of-plane direction. In order to trigger buckling, out-of-plane imperfections were introduced that were equal to 0.001 times the first-mode buckling displacements. The gusset plate sustained a maximum load of 1,606 kN. Strength degradation was measured as the gusset plate buckled and deformed out of plane. Fig. 7(a) shows the finite element model before and at the end of the analysis. The model was supplied with boundary conditions reflecting the test setup, as rigid cylindrical shells (representing the bolts) were displaced in the direction towards the gusset plate. Fig. 7(b) plots the compressive load versus out-of-plane displacement relationship obtained from

three models. The meshing scheme validated from the first study was used, while the number of elements across the thickness of the gusset plate was varied between one and three. The out-of-plane displacement d indicated in Fig. 7(a) is plotted in the abscissa, and the total compressive force applied to the brace member is plotted in the ordinate. Fig. 7(b) indicates that the maximum strength and failure due to instability is represented well by using either two or three elements across the thickness of the gusset plate. Using either model, the measured strength of 1,606 kN was predicted within 10%, while the computed out-of-plane displacement was on the same order as that measured during the test (reported as 25 mm).

Based on the two validation studies, the U10 connection of the I-35W bridge was modeled using C3D8 elements throughout, 16 elements surrounding the bolt holes, and two elements across the thickness of the gusset plates.

Gusset Plate Connection Analysis

The truss forces obtained from the bridge analysis supplied the loading conditions for the detailed, 3D finite element model shown in Fig. 8(a). The concept of the loading condition is shown in Fig. 2(b). The model consisted of five short, stub segments connected through a pair of gusset plates. The dimensions of each component were taken from the original construction drawings (Mn/DOT 2008). A rigid shell plate was attached to the far end of each stub segment and to the top of the upper chords, at the location where the floor truss seated. The vertical load and truss forces were applied to the center of the shell plate, perpendicular to the plate. The truss loading points were allowed to translate only along the original member axis, and the top loading point was restrained from motion in the out-of-plane direction. The transverse reactions computed at the loading points were minimal.

The primary objective of the local model analysis was to examine the stress and strain condition that may lead to the failure shown in Fig. 3. Therefore, the rivet connection was explicitly modeled only between the compression diagonal L9/U10 and the gusset plates. Unlike the other four truss members which were merged to the gusset plate, the diagonal L9/U10 was modeled as an independent element. Force transfer by contact of two elements was permitted only in the direction normal to the surface (In other words, friction was neglected). Rivets were modeled as rigid cylindrical shells interacting with the periphery of the rivet holes. A uniform pressure of 56.5 MPa was applied at both sides of the riveted joint within an annular region of 7.6 mm from the edge of holes to produce a pre-tension of 44.5 kN. This pre-tension is equivalent to the minimum bolt-pretension specified by the Research Council on Structural Connections (RCSC 2004). The pressure was needed to prevent separation between the diagonal and the gusset plates during analysis, and it did not lead to a frictional resistance contribution to the connection because friction between the plates was neglected.

Elasto-plastic steel properties for the gusset plate were based on the tension test data provided by Beshah et al. (2008). The relationship between true stress and logarithmic plastic strain for the gusset plate was approximated as a piecewise linear line with 355 MPa at 0 plastic strain, 517 MPa at 0.04, and 607 MPa at 0.1. The meshing strategy was based on the study described in previous section. The model had a total of 119,932 elements and 200,753 nodes. Computations were run on an IBM Power4 system at the University of Minnesota Supercomputing Institute.

The analysis was conducted in five successive steps designated below. The truss forces were increased in four steps, by first introducing the forces for Case 1 of the bridge analysis (Step 1), and increasing the forces, in order, to Case 2 (Step 2), Case 3 (Step 3), and Case 4

(Step 4). Subsequently, a linear thermal gradient of $17\text{ }^{\circ}\text{C}$ was introduced between the surfaces of the two gusset plates by either maintaining the same support conditions (Step 5a) or freezing translation of the five truss loading points (Step 5b). In truss bridges, the truss members are supplied with substantial longitudinal restraint by surrounding members (Huckelbridge 2008). The two support conditions should provide reasonable bounds for the expected restraints.

Analysis Results

Fig. 9(a) shows a photographic view of the fracture observed along the compression diagonal L9/U10 (fracture (A) in Fig. 3(b)). Fig. 9(b) shows the maximum principal stress field in the gusset plate, near the same perimeter rivet holes, evaluated at completion of analysis Step 4. On the left edge of the perimeter rivet holes, the maximum principal stress acts in the vertical direction. The direction agrees well with the fracture seen in Fig. 9(a), and indicated by dotted lines in Fig. 9(b). Therefore, it is suspected that fracture initiated on the left edge of the holes (as viewed in Fig. 9) due to large normal stresses, and propagated straight until the fracture grew large enough to disturb the stress field and change the direction of fracture propagation. The comparison in Fig. 9 indicates that the nonlinear analysis procedure and detailed local model may provide important insight of the gusset plate failure. In this study, the initiation of fracture is not quantified. The critical stress and strain values depend substantially on the meshing scheme, as demonstrated in Fig. 6.

Fig. 10 shows how yielding of the gusset plates spread as the analysis progressed. The grey to black color indicates the region where the Mises stress exceeds the specified yield stress of 355 MPa. The region in white is elastic. At the end of Step 1, localized plasticity was observed adjacent to the upper-left corner of the compression diagonal L9/U10 surrounding rivet holes. Additionally, a small region below the upper chords yielded because of the large net shear

force along the horizontal section. At the end of Step 2, the yielded region was spread extensively. This result suggests that the dead loads added after the original construction stressed the gusset plates beyond a generally accepted level. The standard practice (Kulicki et al. 2006) is to assure that gusset plates remain elastic under design loads. As the analysis progressed with increasing load and truss forces, yielding spread along the perimeter of the compression diagonal L9/U10 and the lower edge of the upper chords. While the difference between Steps 4 and 5a are barely noticeable, Step 5b clearly produced an increased area of yielding beyond Step 4. The regions of high stresses coincide with the reported locations of fracture, (A) and (B) in Fig. 3(b). The substantial yielding shown in Fig. 10 may have led to failure of the gusset plate.

Fig. 11 plots the Mises stress versus equivalent plastic strain (PEEQ) measured at a sampling point (dashed line). As indicated in Fig. 10, the sampling point is adjacent to an upper-left rivet hole, and was identified as a critical point where large compressive stresses develop. For uniaxial loading cases, the relationship between Mises stress and PEEQ coincides with the true stress versus logarithmic plastic strain material model (solid line). Therefore, Fig. 11 is also a confirmation that the computed stress and strain field agrees with the assumed material plasticity model (piecewise-linear line in the figure). At the end of Step 1, the sample point is already yielded. At the end of Step 4, the Mises stress was as high as 552 MPa and the PEEQ was 0.07. The PEEQ was increased by 0.02 between Steps 1 and 2, and between Steps 3 and 4. In other words, loads DL2 and CL produced substantial plastic strains in the gusset plate. The increase in stress and PEEQ caused by temperature gradient was greater than the increase from live loads (LL) but less substantial than that due to the construction loads (CL). The PEEQ produced by the sum of all loading effects was roughly 0.08.

Fig. 11 also shows data (triangles) obtained from analysis with ABAQUS after increasing the gusset plate thickness from 13 mm to 25 mm, the latter which would satisfy current design requirements. Although the thicker gusset plate also yielded at the end of Step 1, the PEEQ at the sampling point at the end of Step 4 was smaller than 0.01. Very limited yielding was observed in the thicker gusset plates, except in a very limited region including the sampling point. Such limited yielding is accepted in steel connection design. Therefore, the thicker gusset plates would have sustained the same load conditions without discernable yielding.

The above analysis results, combined with the fracture study by the NTSB (2008a), suggest that failure of gusset plate U10 initiated either along the perimeter of the compression diagonal (fracture (A) in Fig. 3(b)) or along the critical shear plane below the upper chords (fracture (B)). The location of yielding suggests that interaction of shear force and compression may have influenced the failure. The interaction is not expected to lead to potentially dangerous conditions of properly sized gusset plates. However, it is worthwhile to consider the compression-shear interaction for the undersized U10 gusset plates. To this end the local model analysis was repeated for a modified gusset plate connection shown in Fig. 8(b) that replaces the top chord U9/U10 and vertical U10/L10 by fixed edge supports. This connection is a compression connection, unlike the U10 connection which is subjected to combined shear and compression, but resembling the specimens studied by Yam and Cheng (1993). However, due to the short unsupported edges of the gusset plate, buckling should not be a concern for this compression connection.

Fig. 12 compares the response obtained from the two connection models, the U10 connection shown in Fig. 8(a) and the compression connection shown in Fig. 8(b). The response is represented by the compression in L9/U10, incremented according to Steps 1 to 4, against the

averaged strain of gauge length L indicated in the figure. The elastic stiffness was 40% smaller for the U10 connection compared to the compression connection. Although the U10 connection softened progressively as the compression exceeded 7,500 kN, the compression connection remained largely elastic when the analysis was terminated at a compression of 11,120 kN. The U10 connection was affected substantially by yielding in the region in front of the connection. Figures 10 and 12 suggest that, beyond Step 1, the stress was redistributed from the front of the connection to the shear lines along the perimeter rivet holes, resulting in the wide yielded region surrounding member L9/U10. Discernable yielding did not occur in the compression connection at the end of Step 4.

Standard design procedures (Holt and Hartmann 2008; Kulicki et al. 2006) check the compressive strength and shear strength independently, but do not check the interaction between the forces. On the other hand, results from this study suggest that shear-compression interaction contributed to the substantial yielding of the gusset plates, and therefore, may have played a key role in the I-35W Bridge collapse.

Buckling sensitivity studies were conducted to address the pre-collapse deformed configuration of the gusset plates, but are not shown here for brevity. These studies included the use of imperfections to define the initial configuration of the U10 gusset plates (using the first buckling mode shape with various amplitudes), as well as analyses in which the gusset plates were initially deformed (in a pattern simulating the first buckling mode and with a peak amplitude of 12.7 mm). The former case is stress/strain free prior to load application, whereas the latter introduces stress and strain fields in response to the deformed shape. These studies indicated only minor sensitivity to the initial imperfections/deformed shapes, with the relation

between Mises stress and PEEQ being nearly identical. These results agree, in part, with the NTSB study (2008d) which suggested a greater influence of buckling on the gusset plate failures.

Conclusions

Reported evidence suggests that the collapse of the I-35W Bridge initiated at the U10 gusset plate connections. These connections were analyzed using detailed finite element models. The forces applied on the gusset plate connections were estimated carefully based on construction drawings and other available information. The computed stress and strain fields were compared against the patterns of fracture observed after the bridge collapse. Key findings are summarized as follows:

- The concrete deck overlay and new parapets added in later years after original construction increased the dead loads by 30%.
- The live loads were rather small at the time of collapse because of the traffic lane closures.
- The construction material and equipment placed on the day of collapse caused substantial increase in the forces applied on the U10 gusset plates.
- Temperature gradient between the two sides of the connection may have produced additional stress and strain in the gusset plates. However, the effect of temperature gradient is difficult to quantify because the computed results are highly dependent on the assumed boundary conditions for the analysis model.
- A substantial portion of the U10 gusset plates may have been yielded at the time of collapse. Weight increase due to past deck reconstruction and construction material and equipment staged on the day of collapse, along with insufficient strength of the gusset plate, were

identified as the main contributing factors to the substantial yielding. These results corroborate the findings by the NTSB (2008d) and Hill et al. (2008).

- Interaction between compression and shear may have played an important role in the gusset plate failure and further study of this phenomenon is needed.

Acknowledgements

This project was supported by the National Science Foundation (CMMI-0753666) and by the Center of Transportation Studies of the University of Minnesota. Computing resources were provided by the Minnesota Supercomputing Institute.

Accepted Manuscript
Not Copyedited

References

- American Association of State Highway Officials (AASHTO). (1973). *Standard specifications for highway bridges, 11th edition*. Association General Offices, AASHTO, Washington, D.C.
- Beshah, F., Wright, W., and Graybeal, B. (2008). “Mechanical property test report (I-35W over the Mississippi River).” *Federal Highway Administration Turner-Fairbank Highway Research Center Report*. <<http://www.nts.gov/dockets/highway/hwy07mh024/404089.pdf>> (Dec. 22, 2008).
- Bjorhovde, R. and Chakrabarti, S.K. (1985). “Tests of full-scale gusset plate connections” *J. Struct. Eng.*, ASCE, 111(3), 667-684.
- Chambers, J.J. and Ernst, C.J. (2005). “Brace Frame Gusset Plate Research Phase I Literature Review,” Department of Civil and Environmental Engineering, University of Utah, Salt Lake City, Feb.
- Computers and Structures, Inc. (CSI). (2007). *Basic Analysis Reference Manual*. Berkeley, CA.
- Gross, J. L. (1990). “Experimental study of gusseted connections.” *Eng. J.*, AISC, 27(3), 89-97.
- Hardash, S. G., and Bjorhovde, R. (1985). “New design criteria for gusset plates in tension.” *Eng. J.*, AISC, 22(2), 77-94.
- Hill, H. J., McGormley, J. C., Koob, M. J., and Nugent, W. J. (2008). “I-35W Bridge over the Mississippi River: collapse investigation – Bridge No. 9340, Minneapolis, Minnesota.” *Final Report*, Wiss, Janney, Elstner Associates, Inc., Northbrook, IL, prepared for Mn/DOT. <<http://www.nts.gov/dockets/highway/hwy07mh024/404995.pdf>> (Dec. 22, 2008).

- Holt, R., and Hartmann, J. (2008). "Adequacy of the U10 gusset plate design for the Minnesota bridge No. 9340 (I-35W over the Mississippi River) – Final Report." *Federal Highway Administration Turner-Fairbank Highway Research Center Report*.
<<http://www.nts.gov/dockets/highway/hwy07mh024/404084.pdf>> (Dec. 22, 2008).
- Huckelbridge, A., personal communication, Sep. 15, 2008.
- Kulicki, J. M., Prickett, J. E., and LeRoy, D. H. (2006). "Chapter 13. Truss bridges." *Structural Steel Designer's Handbook, 4th Edition*. Edited by Brockenbrough, R. L. and Merritt, F. S., ASCE, McGraw-Hill Professional, 2006.
- Liao, M (2009). "A Computational Study of the I-35W Bridge Failure." M.S. Thesis, University of Minnesota-Twin Cities, Department of Civil Engineering, May.
- Minnesota Department of Transportation (Mn/DOT). (2008). "I-35W Bridge original plans & details." <<http://www.dot.state.mn.us/i35wbridge/history.html>> (Dec. 22, 2008).
- National Transportation Safety Board (NTSB). (2007). "Loads on the bridge at the time of the accident" *Modeling Group Study Report No. 07-115*.
<<http://www.nts.gov/dockets/highway/hwy07mh024/385259.pdf>> (Dec. 22, 2008).
- National Transportation Safety Board (NTSB). (2008a). "Materials laboratory factual report." *Report No. 07-119*. <<http://www.nts.gov/dockets/highway/hwy07mh024/386200.pdf>> (Dec. 22, 2008).
- National Transportation Safety Board (NTSB). (2008b). "Structural investigation group chairman factual report." *Report No. 08-015*.
<<http://www.nts.gov/dockets/highway/hwy07mh024/387408.pdf>> (Dec. 22, 2008).

National Transportation Safety Board (NTSB). (2008c). *Photos of I-35W Bridge*.

<<http://www.nts.gov/dockets/highway/hwy07mh024/387406.pdf>> (Dec. 22, 2008).

National Transportation Safety Board (NTSB). (2008d). "Modeling group chairman final report." *Report No. 08-119*.

<<http://www.nts.gov/dockets/highway/hwy07mh024/405446.pdf>> (Dec. 22, 2009).

National Transportation Safety Board (NTSB). (2008e). "Collapse of I-35W Highway Bridge, Minneapolis, Minnesota, August 1, 2007." *Accident Report NTSB/HAR-08/03*.

<<http://www.dot.state.mn.us/i35wbridge/ntsb/finalreport.pdf>> (Feb. 22, 2008).

Research Council on Structural Connections (RCSC). (2004). "Specification for structural joints using ASTM A325 or A490 bolts." RCSC, AISC, Chicago, IL.

Simulia (2008). *ABAQUS Version 6.8 Documentation Collection*, Simulia Corp., Dassault Systèmes, Providence, Rhode Island.

Tajima, J., Shimokawa, H., Takena, K., Miki, C., and Ito, F. (1982). "Fatigue tests of truss made of 600 MPa and 800 MPa class steels." *Doc. XIII-1042-82*, International Institute of Welding.

Thornton, W. A. (1984). "Bracing connections for heavy construction." *Eng. J.*, AISC, 21(3), 139-148.

URS Corp. (2006). "Fatigue evaluation and redundancy analysis – Bridge No. 9340 (I-35W over Mississippi River)." *Bridge 9340 Study*, Prepared by URS Corp. for Mn/DOT, Minneapolis, MN.

Whitmore, R. E. (1952). "Experimental Investigation of Stresses in Gusset Plates. Bulletin No. 16, University of Tennessee Engineering Experiment Station.

Yam, M. C. H., and Cheng, J. J. R. (1993). "Experimental investigation of the compressive behavior of gusset plate connections." *Struct. Eng. Rep. No. 194*, University of Alberta, Alberta, Canada.

Yamamoto, K., Akiyama, N., and Okumura, T. (1985). "Elastic analysis of gusseted truss joints." *J. Struct. Eng.*, ASCE, 111(12), 2545-2564.

Yamamoto, K., Akiyama, N., and Okumura, T. (1988). "Buckling strengths of gusseted truss joints." *J. Struct. Eng.*, ASCE, 114(3), 575-590.

Accepted Manuscript
Not Copyedited

List of Tables

Table 1. Loads applied on panel points. (Units in kN).

Table 2. Truss forces at U10. (Units in kN).

Accepted Manuscript
Not Copyedited

List of Figures

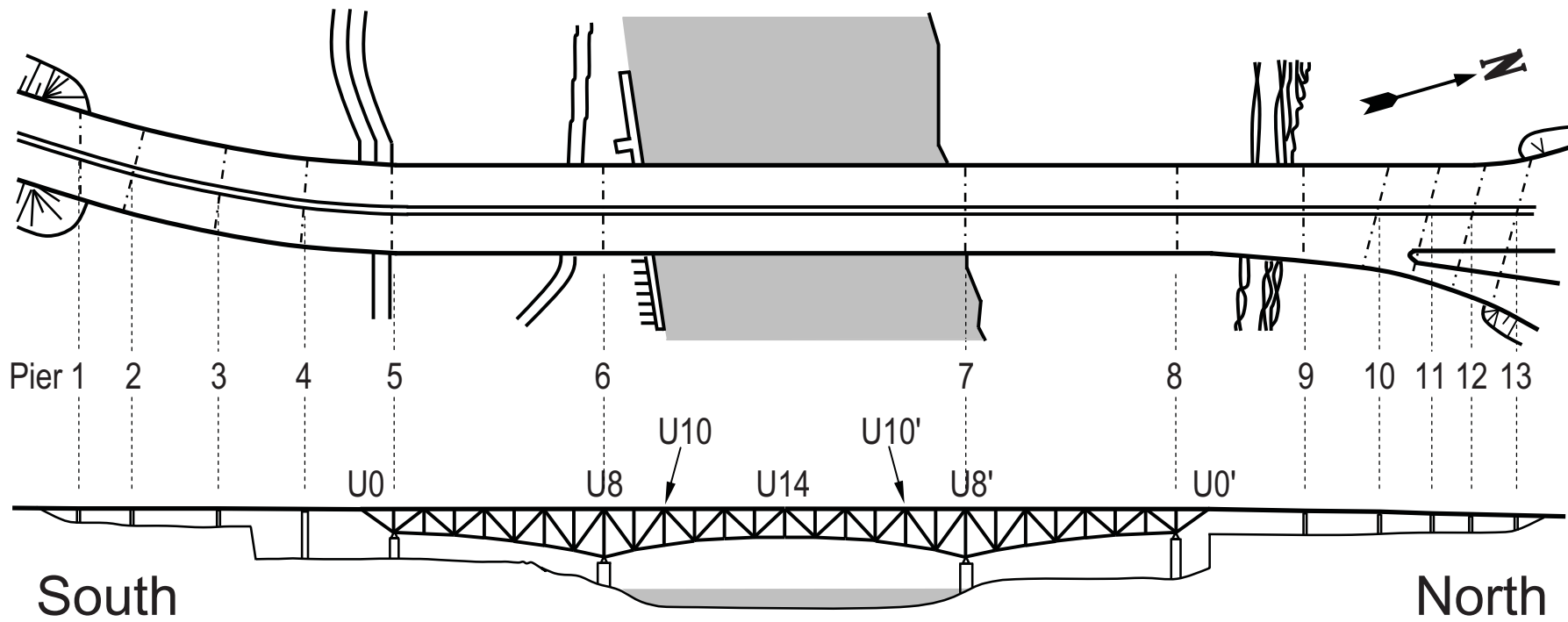
- Fig. 1.** Plan and elevation of I-35W Bridge (based on Mn/DOT 2008).
- Fig. 2.** Panel point U10: (a) photograph of U10W before collapse (from NTSB 2008c); and (b) member designation and truss forces. (Units in kN).
- Fig. 3.** Panel point U10 after collapse: (a) photograph of U10W (from NTSB 2008c); and (b) reported locations of fracture.
- Fig. 4.** Influence lines of truss forces in L9/U10 and U10/L11.
- Fig. 5.** Tension gusset plate connection: (a) photograph of plate after testing (Hardash and Bjorhovde 1985, with permission from AISC); (b) finite element models; and (c) deformation and Mises stress distribution.
- Fig. 6.** Verification for tension gusset plate connection: (a) loading curve; (b) normal stress distribution; and (c) PEEQ distribution.
- Fig. 7.** Verification for compression gusset plate connection: (a) finite element model before and after deformation; and (b) load versus out-of-plane displacement.
- Fig. 8.** Gusset plate connection models: (a) panel point U10; and (b) compression connection.
- Fig. 9.** Fracture along L9/U10: (a) observed fracture; and (b) distribution of maximum principal stress.
- Fig. 10.** Yielding of the gusset plate at the end of (a) Step 1; (b) Step 2; (c) Step 3; (d) Step 4; (e) Step 5a; and (f) Step 5b.

Fig. 11. Mises stress versus PEEQ at a critical point

Fig. 12. Load versus averaged strain measured for sampling gauge

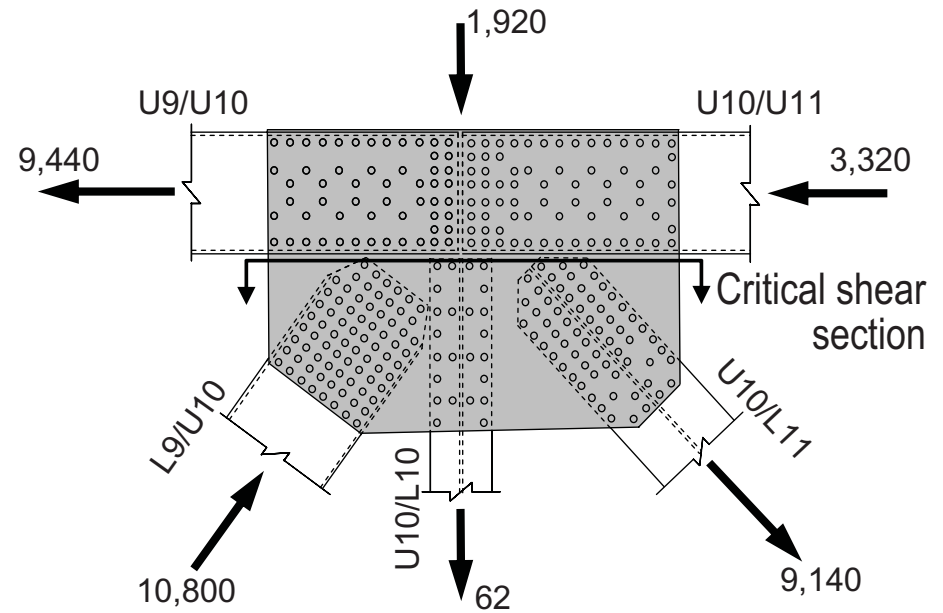
Accepted Manuscript
Not Copyedited

Fig. 1



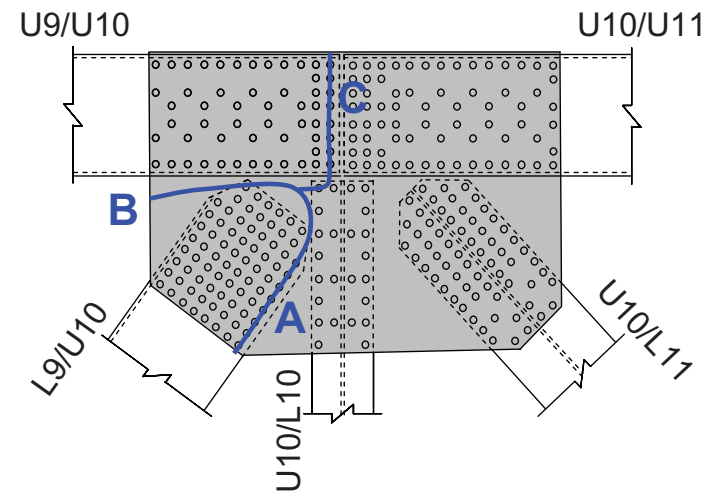
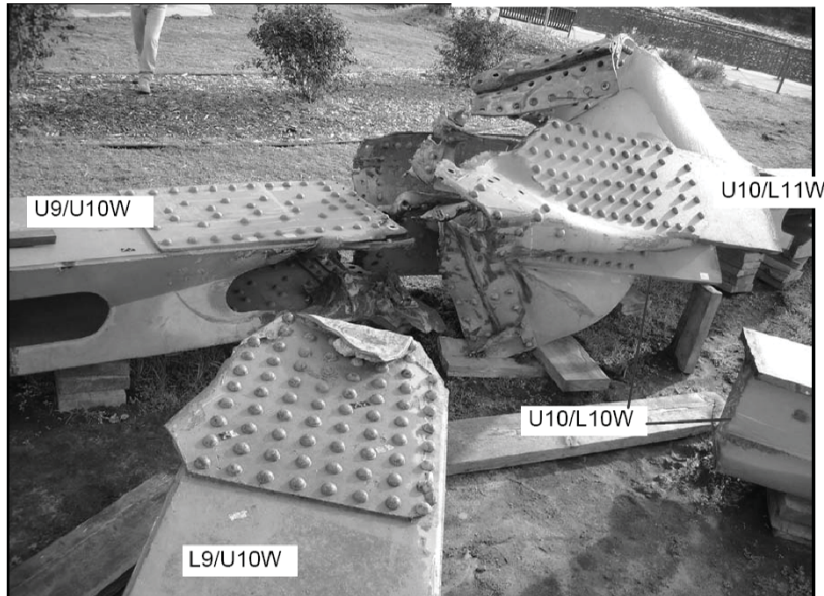
Accepted Manuscript
Not Copyedited

Fig. 2



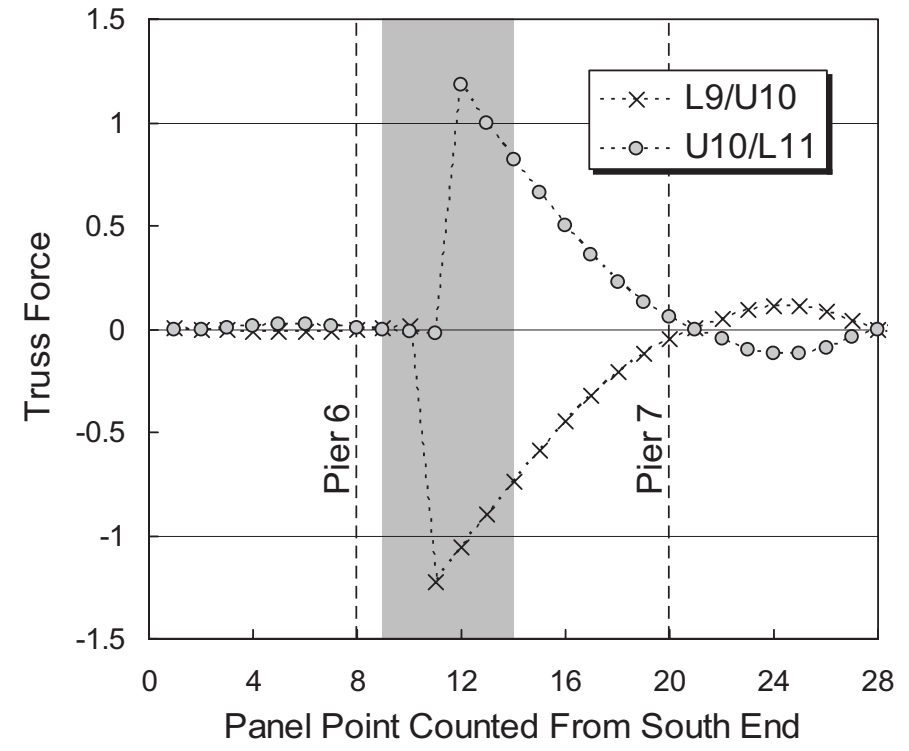
Accepted Manuscript
Not Copyedited

Fig. 3

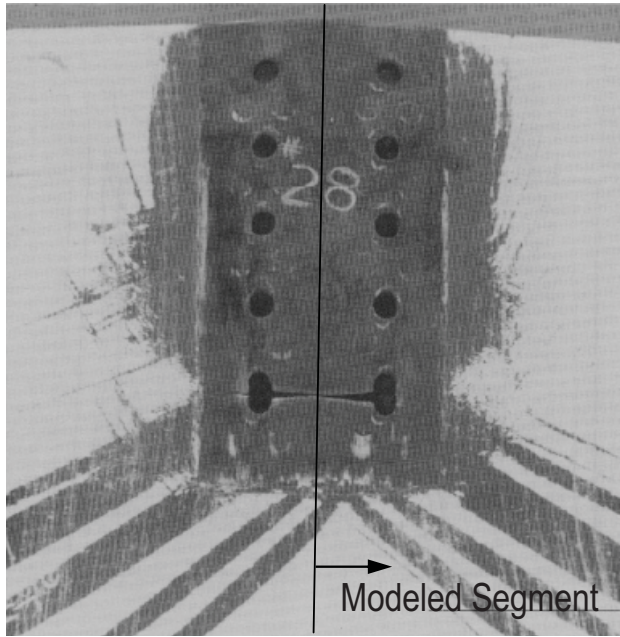


Accepted Manuscript
Not Copyedited

Fig. 4

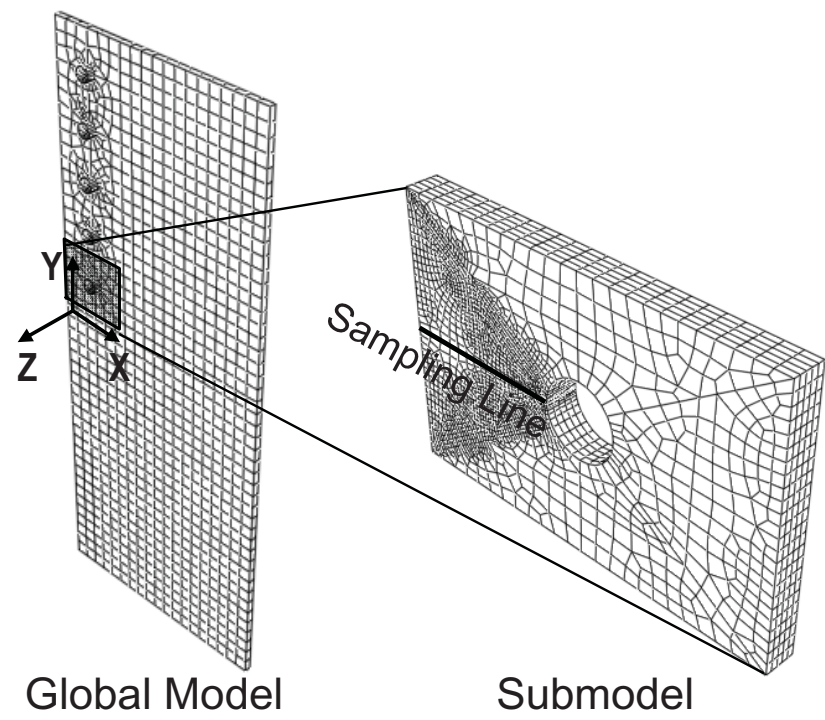


Accepted Manuscript
Not Copyedited

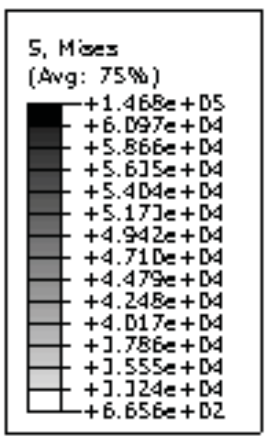


(a)

Fig. 5



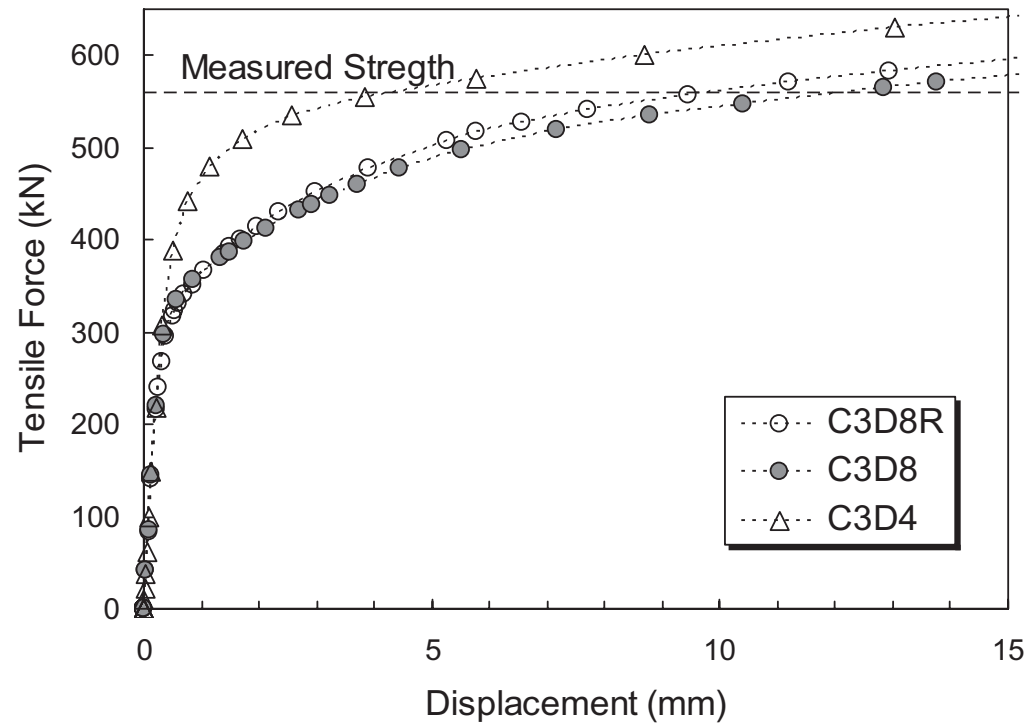
(b)



(c)

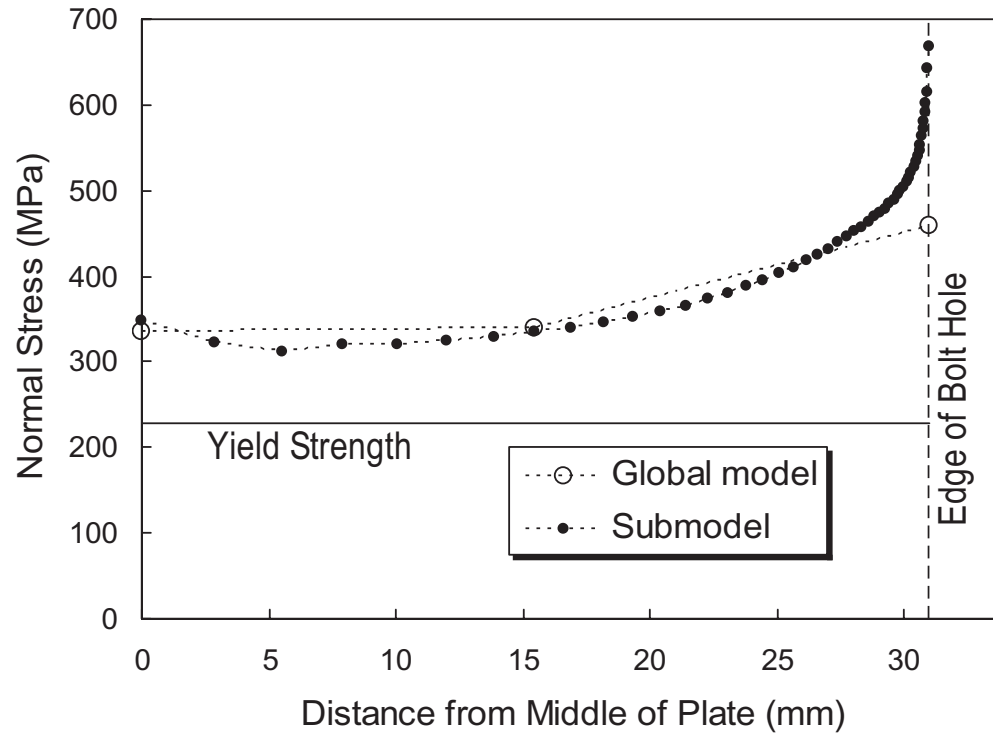
Accepted Manuscript
Not Copied

Fig. 6(a)

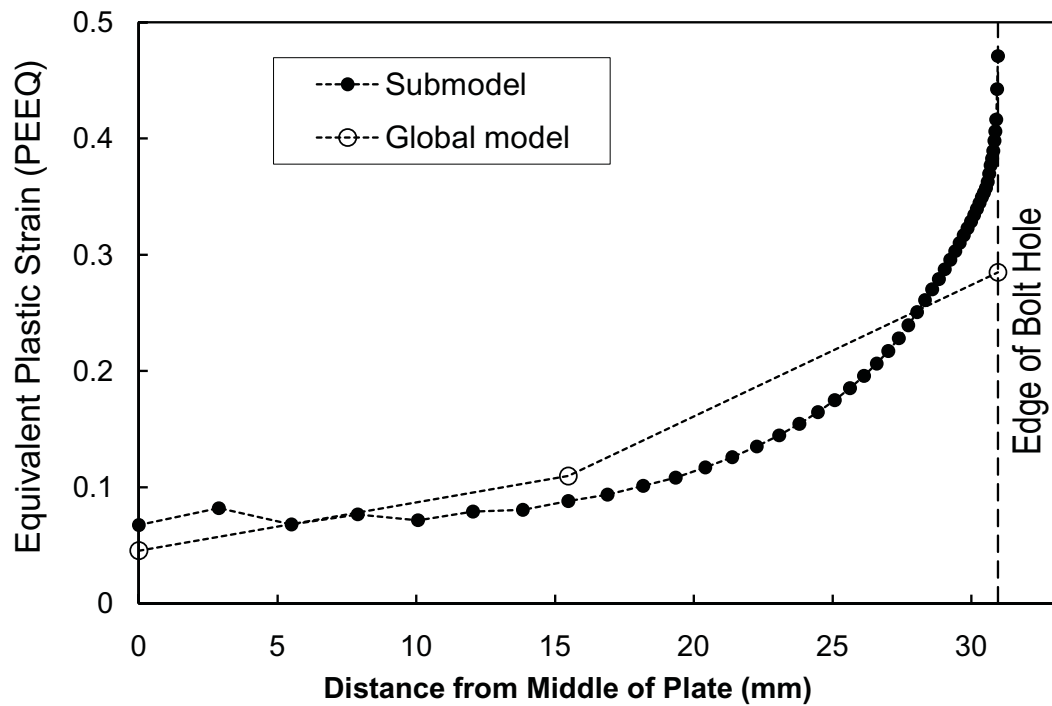


Accepted Manuscript
Not Copyedited

Fig. 6 (b)

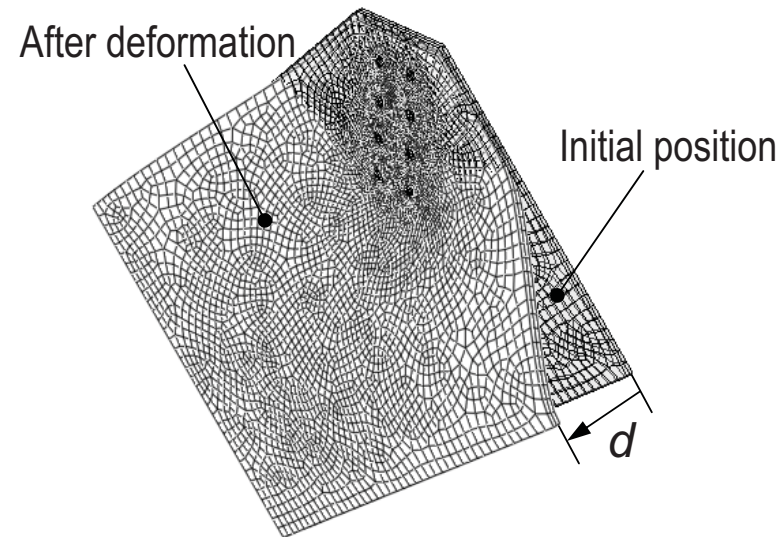


Accepted Manuscript
Not Copyedited

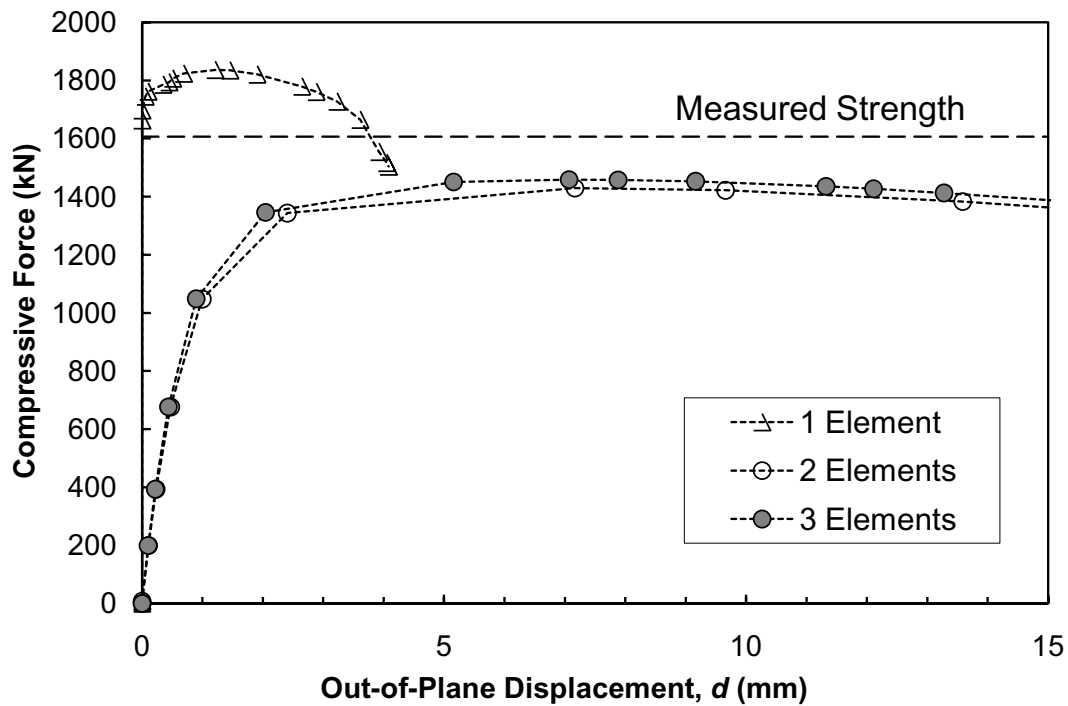


Accepted Manuscript
Not Copyedited

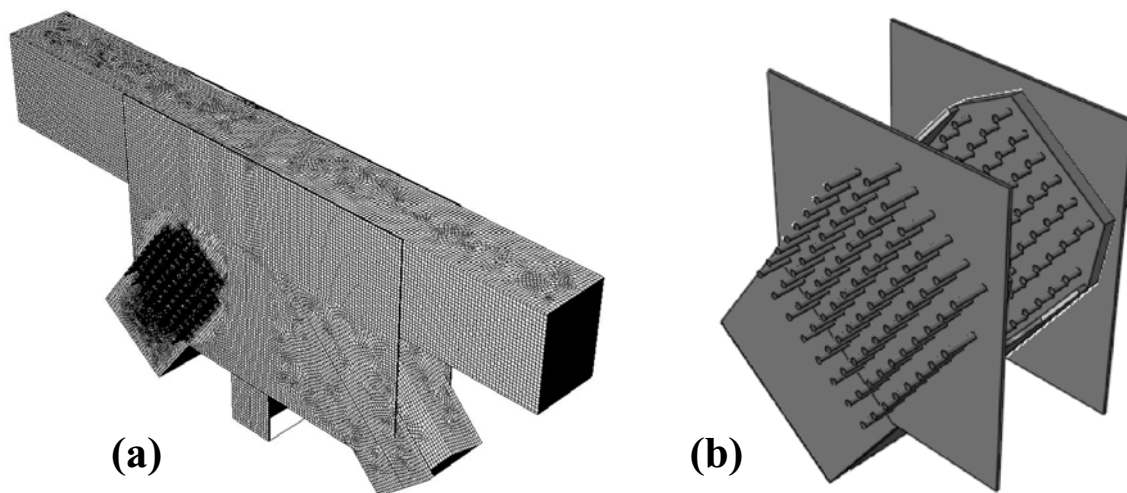
Fig. 7(a)



Accepted Manuscript
Not Copyedited

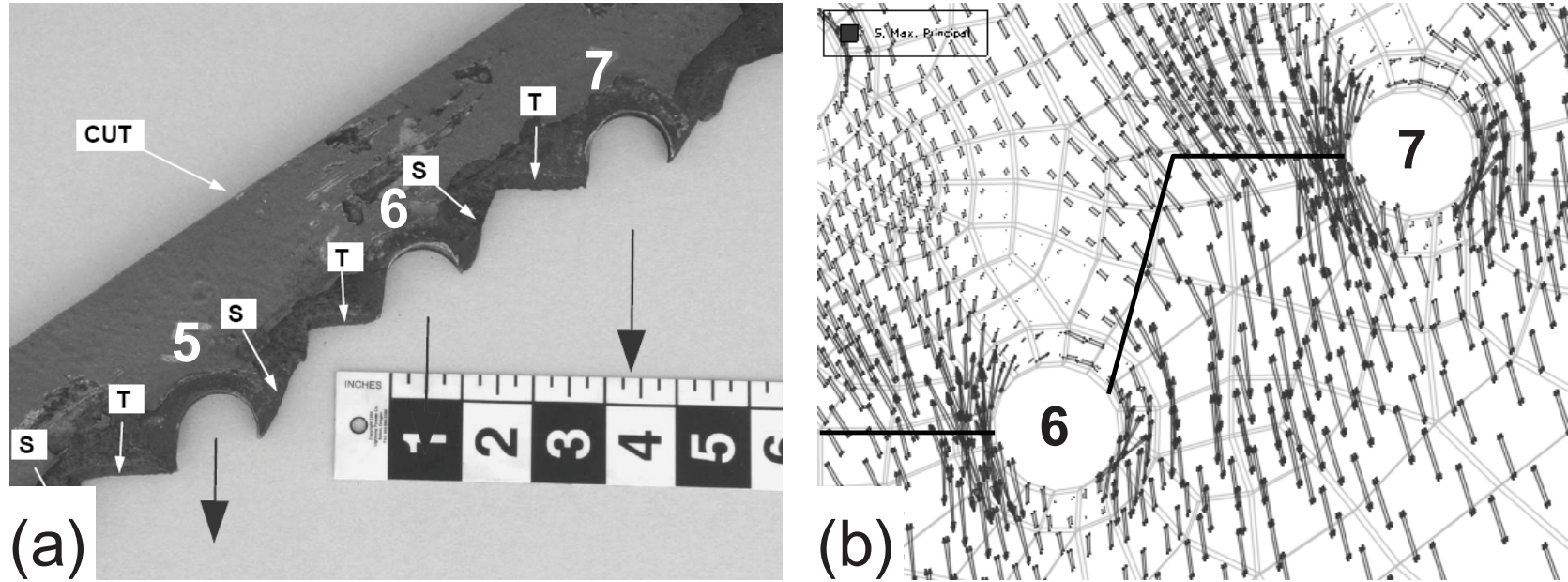


Accepted Manuscript
Not Copyedited



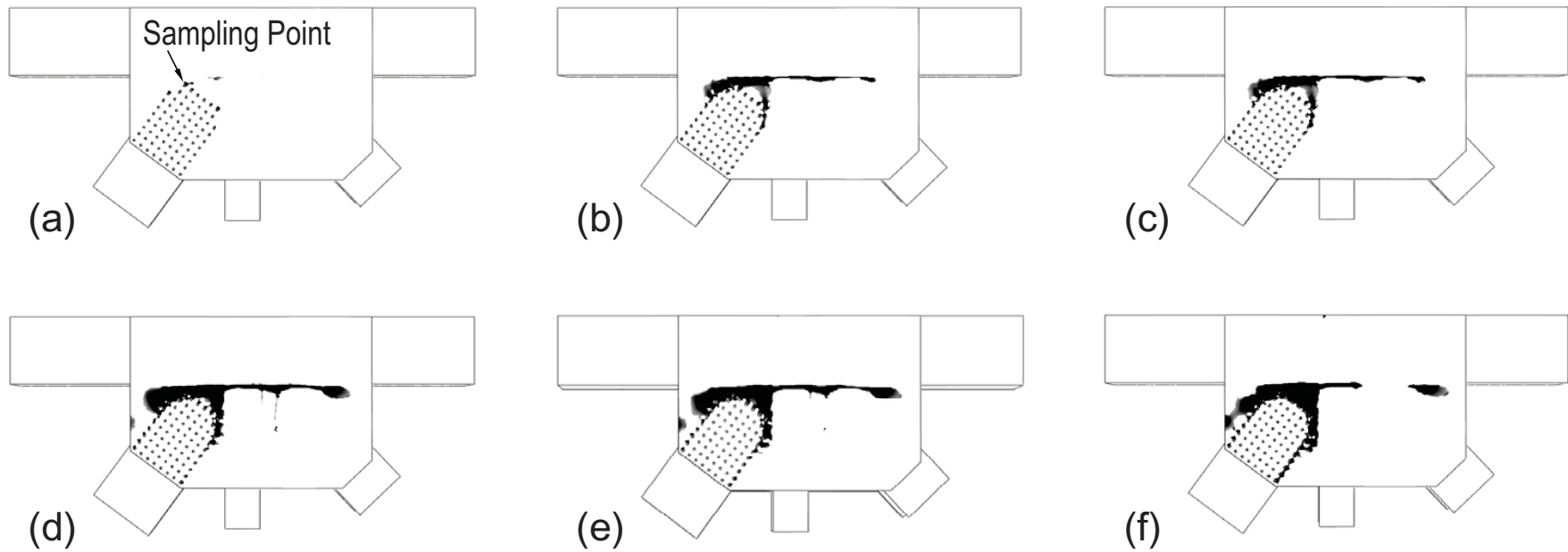
Accepted Manuscript
Not Copyedited

Fig. 9



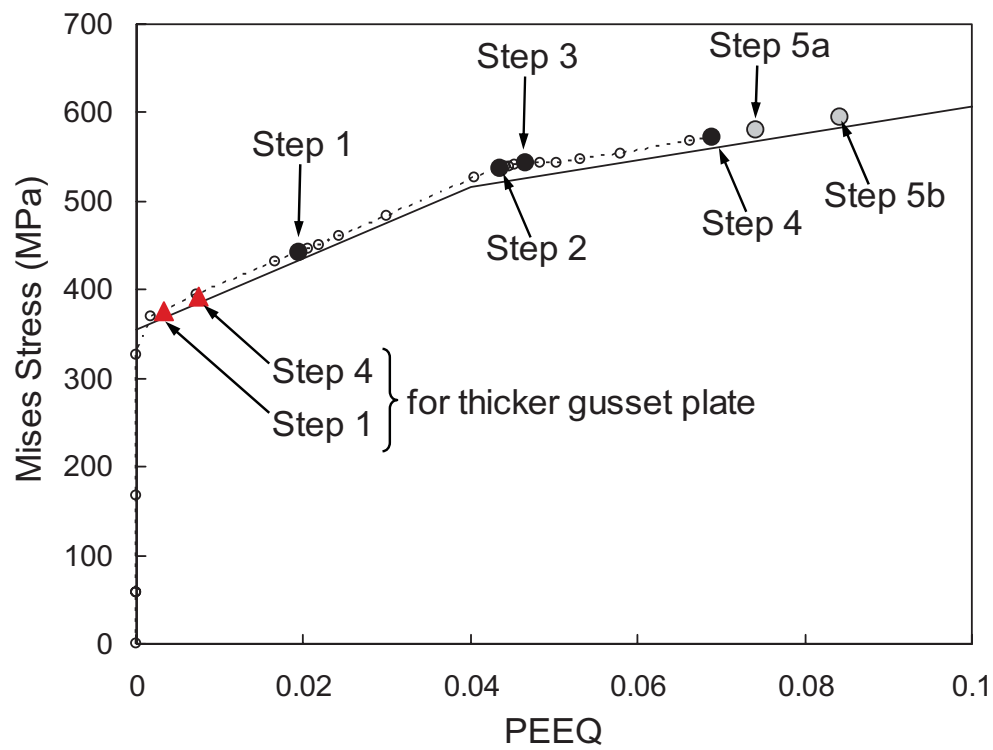
Accepted Manuscript
Not Copyedited

Fig. 10



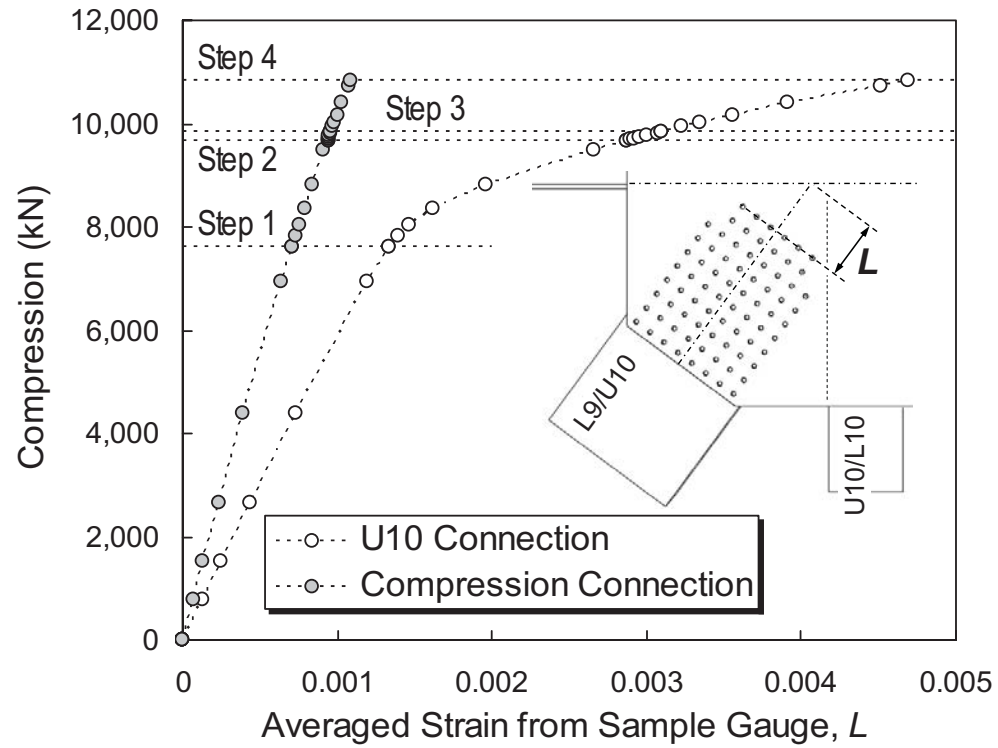
Accepted Manuscript
Not Copyedited

Fig. 11



Accepted Manuscript
Not Copyedited

Fig. 12



Accepted Manuscript
Not Copyedited

Table 1. Loads applied on panel points. (Unit in kN).

Panel point	DL1	DL2	LL	CL
U0	1,868	449	66	0
U1	1,178	389	68	0
U2	1,193	389	68	0
U3	1,188	389	68	0
U4	1,441	389	68	0
U5	1,190	389	68	0
U6	1,219	389	68	0
U7	1,212	389	68	0
U8	1,468	389	48	0
U9	1,206	389	28	260
U10	1,210	389	28	290
U11	1,196	389	28	334
U12	1,189	389	28	180
U13	1,182	389	28	143
U14	1,433	389	28	16
U13'-U9'	Symmetric	Symmetric	Symmetric	0
U8'	1,468	389	28	0
U7'-U1'	Symmetric	Symmetric	26	0
U0'	2,769	733	82	0

Accepted Manuscript
Not Copyedited

Table 2. Truss forces at U10. (Unit in kN).

Member	Original design		Bridge model analysis					
	Case 1	Demand	Case 1	Case 2	Case 3	Case 4	Case T1	Case T2
U9/U10	6,899	9,550	7,060	8,960	9,210	9,440	10	-1,500
U10/U11	-2,162	-4,110	-2,020	-2,540	-2,490	-3,320	12	-1,170
L9/U10	-7,473	-10,177	-7,620	-9,670	-9,830	-10,800	2	246
U10/L11	6,370	8,785	6,560	8,310	8,440	9,140	-2	-273
U10/L10	1,205	2,402	62	62	62	62	0	0

Accepted Manuscript
Not Copyedited